Expansion-history preferences of DESI DR2 and external data

Prakhar Bansal^{®*} and Dragan Huterer^{®†}

Department of Physics and Leinweber Center for Theoretical Physics, University of Michigan, 450 Church St, Ann Arbor, Michigan 48109

(Received 13 February 2025; accepted 4 June 2025; published 15 July 2025)

We explore the origin of the preference of Dark Energy Spectroscopic Instrument (DESI) Data Release 2 (DR2) baryon acoustic oscillation measurements and external data from cosmic microwave background (CMB) and type Ia supernovae (SNIa) that dark energy behavior departs from that expected in the standard cosmological model with vacuum energy (Λ CDM). In our analysis, we allow a flexible scaling of the expansion rate with redshift that nevertheless allows reasonably tight constraints on the quantities of interest, and adopt and validate a simple yet accurate compression of the CMB data that allows us to constrain our phenomenological model of the expansion history. We find that data consistently show a preference for a 3%–4% increase in the expansion rate at $z \simeq 0.7$ relative to that predicted by the standard Λ CDM model, in excellent agreement with results from the less flexible (w_0, w_a) parametrization which was used in previous analyses. Even though our model allows a departure from the best-fit Λ CDM model at zero redshift, we find no evidence for such a signal. We also find no evidence (at greater than 1σ significance) for a departure of the expansion rate from the Λ CDM predictions at higher redshifts for any of the data combinations that we consider. Overall, our results strengthen the robustness of the findings using the combination of DESI, CMB, and SNIa data to dark-energy modeling assumptions.

DOI: 10.1103/zypq-s6nl

I. INTRODUCTION

Recent constraints on dark energy [1,2] from the Dark Energy Spectroscopic Instrument (DESI [3,4]) and external data have provided a preference—though not yet firm evidence—for dynamical dark energy. Adopting the popular parametrization of the equation of state of dark energy $w(a) = w_0 + w_a(1-a)$ [5,6], where w_0 and w_a are free parameters and a is the scale factor, the analysis of DESI data, combined with cosmic microwave background (CMB) and type Ia supernovae (SNIa) favor values with $w_0 > -1$ and $w_a < 0$, and depart from the standard cosmological model with vacuum energy ($w_0 = -1$, $w_a = 0$) at the statistical level between 2.7σ and 4.2σ [2].

One interesting feature implied by the combined analysis of DESI and external data in the w_0w_a CDM model [1] and some alternative parametrizations [7,8] is that dark energy starts out "phantom" [with w(z) < -1] at high redshift, and crosses into the w(z) > -1 regime at $z \lesssim 1$. This at face value implies two anomalies not expected in the standard Λ CDM model: 1) a dark energy density that increases in time (in the phantom regime at higher redshifts), but also 2) dark energy density that subsequently *decreases* in time [in the w(z) > -1 regime]. Much has been written

*Contact author: prakharb@umich.edu †Contact author: huterer@umich.edu about these results, with the emphasis on alternative parametrizations of the dark energy sector that allow more degrees of freedom [9–11], explorations of modified-gravity fits to the data [12,13], relation to neutrino-mass constraints [14,15] and other investigations [16–24]. These studies generally confirmed the aforementioned physical picture obtained in the simple (w_0, w_a) parametrization.

A key question here is whether there is really separate evidence for either w(z) > -1 at lower redshifts or for w(z) < -1 at higher redshifts—or for both. Unfortunately most of the studies carried out thus are not equipped to answer this question, as their rigid parametrizations impose a coherence across redshift and may not have enough probing power to detect statistically significant preferences in the data. For instance, in the (w_0, w_a) model, a preference by data for w(z) > -1 at low redshift, combined with the general preference to return to the ΛCDM value $(w(z) \simeq -1)$ at $z \simeq 1$ in order to fit, e.g., the distance to recombination, guarantees a preference for phantom dark energy at $z \gtrsim 1$ just because of the stiffness of the parametrization. Richer descriptions of the dark-energy sector, including a binned description of the equation of state, are possible, but suffer from large parameter-space degeneracies, and consequently poor constraints. Another, very different, approach discussed in the community was removing individual data points (in, e.g., DESI's measured distances) and seeing how the constraints change, but this is a very inefficient way to understand what the data are really

telling us, and specifically *where* the preference for dynamical energy is coming from.

Our goal here is to identify precisely what features in the data are responsible for the preference for dynamical dark energy seen by DESI and external data. To that effect, we choose to consider a piecewise-constant parametrization of the expansion rate H(z). This approach has several advantages: 1) like the equation of state w(z), it too directly propagates into the different kinds of distances probed by DESI data, and communicates the effects of dark energy to SNIa and CMB observables (see the next section for details); 2) unlike any smooth equation-of-state description, direct parametrization of H(z) allows rapid changes in the expansion rate, which is especially useful in understanding preferences shown by the data at low redshift, and 3) despite its flexibility, a binned H(z) prescription does not suffer from large degeneracies and allows us to constrain all model parameters, and the derived distances, to a reasonably good precision. We are reluctant to follow a tiresome and inaccurate tradition and call this method "model independent," but the built-in variation of the expansion rate in multiple redshift bins is the key feature that allows us to understand how different redshift ranges contribute to the results.

II. MODEL AND ANALYSIS METHODOLOGY

We consider a model that modifies the standard Hubble parameter by incorporating perturbative parameters, allowing us to explore deviations from the standard Λ CDM framework across multiple redshift bins. We refer to this model as the modified-H model; it is given by

$$H(z) = H_0^{\text{LCDM}} E(z) (1 + \alpha_i), \tag{1}$$

where $H_0^{\rm LCDM}$ is the Hubble constant in the standard Λ CDM model and α_i are the parameters of the model whose nonzero values allow departures from Λ CDM. We define each α_i to be defined in one of the six redshift bins which approximately coincide with the six DESI DR2 bins into which the Baryon Acoustic Oscillation (BAO) measurements were compressed [1] (see their Table I). The function E(z) is given in its standard Λ CDM form

$$\begin{split} E(z) &= \sqrt{\Omega_{\rm m} (1+z)^3 + \Omega_{\rm R} (1+z)^4 + (1-\Omega_{\rm m} - \Omega_{\rm R})} \\ \Omega_{\rm m} &\equiv \left(\frac{100}{H_0^{\rm LCDM}}\right)^2 (\Omega_{\rm cdm} h^2 + \Omega_{\rm b} h^2), \end{split} \tag{2}$$

where the Hubble constant is in units of km s⁻¹ Mpc⁻¹, $\Omega_{\rm cdm}h^2$ and $\Omega_{\rm b}h^2$ are the physical energy densities in cold

TABLE I. Parameters used in our modified-H analysis and their respective (flat) prior ranges. Note that $H_0^{\rm LCDM}$ is only varied in our $\Lambda {\rm CDM}$ analysis (which we run for comparison and where we also vary $\Omega_{\rm b}h^2$ and $\Omega_{\rm cdm}h^2$); it is fixed to the $\Lambda {\rm CDM}$'s best value in the modified-H analysis. See text for details. The redshift bins for α parameters are defined in *left-closed*, *right-open* intervals.

Parameter	Description	Prior (flat)
$\Omega_{\rm b}h^2$	Physical baryon density	[0.005, 0.1]
$\Omega_{\mathrm{cdm}} h^2$	Physical CDM density	[0.002, 0.20]
H_0^{LCDM}	unmodified Hubble constant	[20, 100]
α_1	$0.0 \le z < 0.4$	[-0.1, 0.3]
α_2	$0.4 \le z < 0.6$	[-0.1, 0.15]
α_3	$0.6 \le z < 0.8$	[-0.1, 0.15]
α_4	$0.8 \le z < 1.1$	[-0.1, 0.1]
α_5	$1.1 \le z < 1.6$	[-0.1, 0.1]
$\underline{\alpha_6}$	$1.6 \le z < 4.16$	[-0.1, 0.1]

dark matter and baryons respectively. Appendix C explains how massive neutrinos contribute to radiation density $\Omega_{\rm R}$, scaling as nonrelativistic matter at low redshifts and becoming progressively more relativistic at high z. In Eqs. (1) and (2), we set $H_0^{\rm LCDM}$ to its best-fit value from the standard Λ CDM analysis with the alpha parameters set to zero, which is about 68 km s⁻¹ Mpc⁻¹, the precise value depending on the data combination used (see the next Section). Moreover, note from Eq. (2) that $\Omega_{\rm m}$ is a derived parameter in our analysis. The transverse and line-of-slight comoving distances are, respectively,

$$D_{\rm M}(z) = c \int_0^z \frac{dz'}{H(z')}; \qquad D_{\rm H}(z) = \frac{c}{H(z)}.$$
 (3)

We assume that the model reverts to standard ΛCDM at redshifts above the highest bin, at z>4.16. No such assumption has been made at low redshift, where H(z=0) is allowed to differ from the ΛCDM value H_0^{LCDM} even at z=0. In particular, the Hubble constant that enters the distances is $H(z=0)=H_0^{\text{LCDM}}(1+\alpha_1)$, which is in general different from the expansion rate that converts from the physical density $\Omega_{\rm m}h^2$ to matter density relative to critical $\Omega_{\rm m}$ [see again Eq. (2)]. This agrees with our logic that both $\Omega_{\rm m}h^2$ and $\Omega_{\rm m}$ are set in the early universe where the unmodified Hubble parameter $H_0^{\text{LCDM}}E(z)$ is relevant.

With all that in mind, there are a total of eight parameters in our analysis: the six alphas, and the physical baryon and CDM densities $\Omega_b h^2$ and $\Omega_{\rm cdm} h^2$, which control the sound horizon as well as enter the lower-redshift distances as in Eq. (1). These parameters and their respective priors in our analysis are given in Table I.

We modify the standard cosmological code CAMB to compute the background quantities like Hubble rate, distances and supernova magnitudes in our modified-H

¹Our binning is identical to that from DESI DR2 [2], except that we extend the lowest bin, which was originally 0.1 < z < 0.4, all the way down to z = 0 in order to allow the Hubble parameter at z = 0 to vary independently of $H_0^{\rm LCDM}$, as well as to take into account the impact of SNIa data at z < 0.1.

model. To obtain the constraints on the cosmological parameters of our model we use the Monte Carlo Markov Chain (MCMC) sampler in Cobaya [25]. For our MCMC chains, we use the default convergence criteria of the Gelman and Rubin R statistic < 0.01. To calculate the means, confidence intervals and likelihood distributions for our model parameters, we use the GetDist [26] code with our converged MCMC chains.

III. DATA

We use the following data:

DESI DR2 BAO. We use the measurements from the DESI Data Release 2 BAO analysis (henceforth DESI DR2 BAO, or just DESI), and adopt the 13 distance measurements, and their covariance, as quoted in Table IV of [2] and validated in supporting DESI DR2 publications [27,28]. To make our analysis as simple and as model independent as possible, we do not use the additional information from the full-shape clustering of DESI sources [29].

Compressed CMB data. It is often very useful to compress the CMB data to a few physically motivated quantities. There are two fundamental reasons for this: first, such compression allows analyses of purely phenomenological models for which a theoretically expected CMB angular power spectrum cannot be computed. And second, the compression also allows a much faster evaluation of the CMB likelihood than a full power-spectrum-based likelihood would. The compression is likely to accurately capture information from dark-energy models that smoothly affect the expansion and growth history.

Following a similar well-established approach (e.g., [30–36]), we compress the CMB into three physical quantities: the "shift" parameter R [30] and the angular location ℓ_a , which are defined as

$$R = 100\sqrt{\Omega_{\rm b}h^2 + \Omega_{\rm cdm}h^2 + \Omega_{\nu,\rm m}h^2}D_{M*}/c$$

$$\ell_a = \pi D_{M*}/r_*, \tag{4}$$

as well as the physical baryon density $\Omega_{\rm b}h^2$. Here D_{M*} and r_* are, respectively, the transverse comoving distance to, and the sound horizon at, the surface of last scattering evaluated at $z_*=1090$. Moreover, $\Omega_{\nu,\rm m}h^2(=\sum m_{\nu}/93.14)$ describes the massive neutrino density; in this work, we have fixed $\sum m_{\nu}$ to 0.06 eV.

We use the combined likelihood from *Planck* and Atacama Cosmology Telescope (ACT). Specifically, we adopt the joint likelihood that makes use of the PR3 *Planck* PLIK likelihood [37] and the Data Release 6 of ACT [38].² The resulting compressed datavector is

$$\mathbf{v}_{\text{CMB}} \equiv \begin{pmatrix} R \\ \ell_a \\ \Omega_b h^2 \end{pmatrix} = \begin{pmatrix} 1.7504 \\ 301.77 \\ 0.022371 \end{pmatrix} \tag{5}$$

and the covariance matrix between these three compressed parameters is given by

$$C_{\text{CMB}} = 10^{-8} \times \begin{pmatrix} 1559.83 & -1325.41 & -36.45 \\ -1325.41 & 714691.80 & 269.77 \\ -36.45 & 269.77 & 2.10 \end{pmatrix}. \tag{6}$$

We find an excellent fit not only for the Λ CDM model on which this compression was derived, but also for the w_0w_a CDM model. We provide the details of this validation in Appendix A.

Type Ia supernovae. Our principal SNIa dataset is the Dark Energy Survey Year 5 Data Release (DESY5 [39]). It contains 1829 SNIa, of which 1635 are photometrically classified objects in the redshift range 0.1 < z < 1.3, complemented with 194 low-redshift SNIa in the range 0.025 < z < 0.1. We also consider two other SNIa datasets (following the same logic in [1]): the Union3 compilation of 2087 SNIa [40], and the PantheonPlus compilation of 1550 spectroscopically confirmed SNIa in the redshift range 0.001 < z < 2.26 [41], many (1363) in common with Union3. In the PantheonPlus analysis, we also impose a z > 0.01 condition to object selection in order to mitigate the impact of peculiar velocities in the Hubble diagram [42]. In all SNIa data combinations, we marginalize analytically over the offset in the Hubble diagram \mathcal{M} which is a nuisance parameter in a cosmological SNIa analysis.

IV. RESULTS

The constraints on the six alpha parameters from the DESI + CMB + DESY5 analysis, marginalized over the baryon and CDM number densities and the Hubble constant, are shown in Fig. 6 in Appendix B, while the corresponding parameter constraints are shown in Table II. The same Appendix also contains more information about our model fitting.

Overall, we find that the modified-H model gives a slightly better fit to the data than the (w_0, w_a) model—not nearly better enough to indicate a *preference* for our more complex model, but sufficiently so to indicate that the model is a good fit to the data. Overall, the alpha parameters are consistent with zero values predicted by Λ CDM, though we observe a modest 2σ deviation from zero in the third alpha parameter.

A more detailed picture can be obtained by looking at the derived constraints on the Hubble parameter and distances, shown in Fig. 1 for the DESI+CMB+DESY5 data combination. We show, from top to bottom, the derived Hubble parameter; the corresponding constraints on the angular-diameter, Hubble, and volume-averaged distance; and

²The likelihood is available from https://github.com/ ACTCollaboration/act dr6 lenslike.

TABLE II. Constraints on the fundamental parameters of our modified-H model in our fiducial analysis of DESI+CMB +DESY5.

Parameter	Constraint
H_0^{LCDM} (value adopted from Λ CDM fit)	68.24 (Fixed)
$\Omega_{ m b} h^2$	0.02240 ± 0.00014
$\Omega_{ m cdm} h^2$	0.1198 ± 0.0011
α_1	-0.0005 ± 0.0060
α_2	0.0097 ± 0.011
α_3	0.033 ± 0.014
$lpha_4$	-0.0045 ± 0.0095
α_5	-0.012 ± 0.012
α_6	-0.0138 ± 0.0071

finally the constraint on the apparent magnitude of SNIa, all as a function of redshift. In all cases, we show constraints relative to their ΛCDM values computed with best-fit parameters from our analysis (i.e., best-fit H_0^{LCDM} and Ω_{m} , effectively); the ΛCDM best-fit values are shown as black dashed lines and centered respectively at either 1 or zero. Note the general agreement of the predictions from our modified-H model with those from ΛCDM . The most noticeable discrepancy between the two is a 3%-4% "bump" in the expansion rate at $z \simeq 0.7$, which integrates to contribute to a trough in the distances as $z \gtrsim 1.6$.

Figure 2 focuses attention on the preferences in the expansion rate provided by the DESI + CMB and DESI + CMB + SNIa data in our modified-H model. Here, we present the expansion rate relative to that of the best-fit ΛCDM model for the combination of DESI DR2 BAO and CMB alone, and also DESI and CMB combined with either one of the three SNIa datasets: DESY5, Union3, and PantheonPlus (so the second panel of Fig. 2 has the same information as the top panel in Fig. 1). We compare our results with those from the (w_0, w_a) parametrization, shown as the red contours in Fig. 2. The preferences from the modified-H model show excellent overall agreement with those from the (w_0, w_a) parametrization, both for the DESI BAO + CMB combination and for the combinations that include supernovae datasets (DESI BAO + CMB + SNIa): both models show preference for the aforementioned \sim 3%–5% bump in the expansion rate at $z \simeq 0.5$ –0.7.

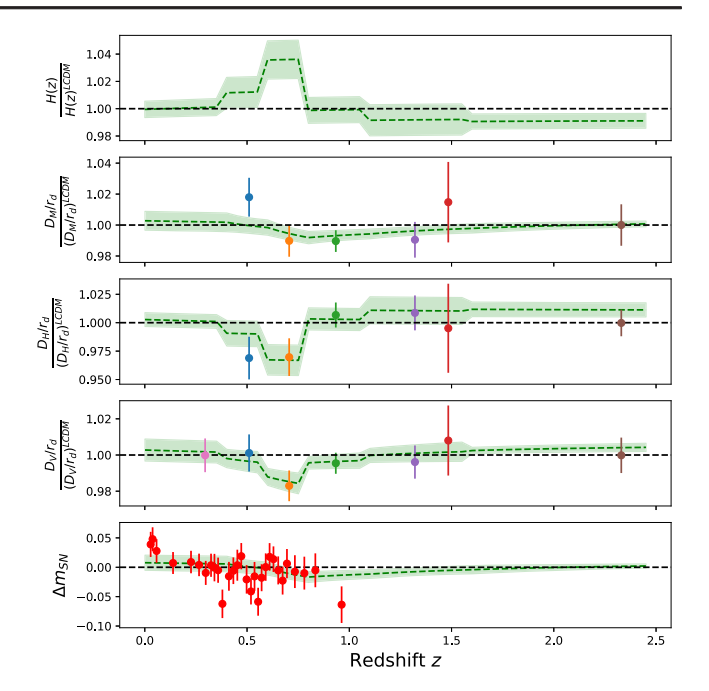


FIG. 1. Constraints from our modified-H model, assuming DESI + CMB + DESY5 data. We show the constraints on the expansion rate H(z) (top panel), followed (in panels that follow, moving down) by the derived constraints on the angular-diameter distance, Hubble distance, and volume-averaged distance all divided by the sound horizon, and finally the apparent magnitude of SNIa. All of the quantities are shown relative to their Λ CDM values computed with best-fit parameters from our analysis. The data points show the DESI DR2 BAO measurements, except in the lowest panel where we show data from SNIa. See text for more details, and in particular the explanation of how SNIa magnitude residuals were defined.

This bump is not particularly significant (being 2.6σ for the DESI BAO + CMB combination, and 2.6σ , 2.7σ , and 2.4σ , respectively, for combinations of DESI and CMB with DESY5, Union3, and PantheonPlus), but it importantly agrees with the same feature in (w_0, w_a) model which does not have the flexibility to cleanly isolate this feature but does have more statistical power due to having fewer parameters. Further, both the modified-H and (w_0, w_a) model show a very mild $(\sim 1\sigma)$ preference for a lower-than-Lambda H(z) at $z \gtrsim 1.5$.

The late-time increase in the expansion rate, if confirmed by future data, would correspond to the corresponding increase in the dark-energy density. Roughly speaking, such an increase could be caused by a "thawing" scalar field [43] that starts to evolve at late times ($z \le 1$) and thus has an equation of state w(z) > -1 and a correspondingly higher density than that in vacuum energy. We do not pursue comparisons with specific dark-energy models further.

One particularly interesting and, to our knowledge, novel result is that all four data combinations shown in Fig. 2 favor the model where H(z) agrees with the Λ CDM

³There is some ambiguity as to how to show SNIa data compared to two theory models (Λ CDM and our modified-H model), given that the Hubble-diagram residuals shown here depend on the Hubble-diagram offset $\mathcal M$ which, however, has already been marginalized over in the analysis. In the bottom panel of Fig. 1, we choose to show the residuals of the best-fit modified-H model relative to best-fit Λ CDM by including the respective values of $\mathcal M$ which we compute by fitting data *after* the best-fit cosmological parameters in the combined DESI + CMB + SNIa analysis have been determined (and fixed). Similarly, we show the data after subtracting the best-fit Λ CDM magnitude and the corresponding $\mathcal M$.

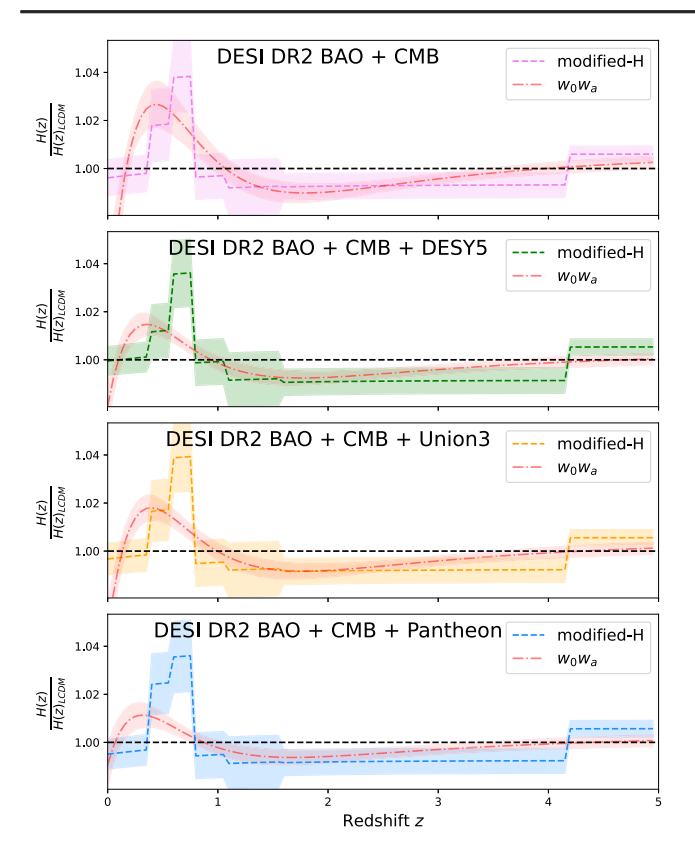


FIG. 2. More detailed view of the H(z) constraint relative to its best-fit value in Λ CDM. We show constraints from DESI BAO and CMB in the first panel (without supernovae), followed by the constraints including one of the three SNIa datasets (DESY5, Union3, and PantheonPlus, respectively, in the second, third, and fourth panels). In each case we show comparison with the corresponding best-fit constraint that assumes the (w_0, w_a) model.

prediction (anchored at high redshift) even at very low redshift, as $z \to 0$. The (w_0, w_a) parametrization does not allow such a variation, since H(z) is affected by a change in w only at first order in z (and comoving distance at second order) [44]; in other words, the value of H(z=0) is completely determined by values of $H_0^{\rm LCDM}$ and $\Omega_{\rm m}$ anchored at high redshift in both the ACDM and $w_0 w_a$ CDM models. In contrast, our parametrization allows a more abrupt, zeroth-order redshift change in H(z). This in principle allows the disagreement between $H(z \rightarrow 0)$ and H_0^{LCDM} in the modified-H model, which the data however do not prefer. It is tantalizing to consider implications of this internal concordance test for direct Hubble-constant measurements that use the astronomical distance ladder, but that will require an in-depth investigation that we leave for near-future work.

Finally, we note that we have done internal checks by changing the details of the binning. We found some dependence of the $\Delta \chi^2$ values on the choice of the binning, but overall results that are consistent with those presented here.

V. CONCLUSIONS

Our principal goal, with the flexible modeling of the expansion history and dark-energy sector given in our Eq. (1), was to give a somewhat more nuanced conclusions on dark energy than constraints from simple parametrizations of the equation of state of dark energy. Assuming the combination of DESI DR2 BAO, compressed Planck and ACT, and SNIa data, we find results remarkably consistent with those from the popular (w_0, w_a) model. We observe a mild preference for the \sim 3%–4% "bump" in the expansion rate at $z \simeq 0.7$ relative to the fit of Λ CDM model to the same data, and a general agreement with findings from ACDM at higher redshift. Moreover, even though we allow variations in the expansion rate at low redshift relative to H(z) anchored at high redshift, we see no evidence for the departure from Λ CDM model's expectation as $z \to 0$.

One might be tempted to criticize our modified-H model as insufficiently "physical," as it allows for sharp transitions in the expansion rate. We think that our model's flexibility, especially one that goes beyond that of smooth w(z) descriptions, is precisely its feature. Given the lack of *any* compelling dark-energy models, it is essential to keep an open mind regarding the description of the dark-energy sector. That is what we have proceeded to do here.

Finally, we have also provided in Appendix A an accurate compression of the CMB (*Planck*+ACT) data, which should prove useful in constraining beyond-standard models of dark energy.

It is becoming clear that a relatively low redshift range, $z \lesssim 0.8$, is becoming very interesting to explore with future and better data. This is where we (with the modified-H model) and previous findings [with the (w_0, w_a) parametrization] consistently see hints of a preference for dynamical dark energy, although this could certainly be just a statistical fluctuation. This is also the redshift range where we rely in good measure on data from SNIa, which are essential in predicting the behavior of dark energy at $z \lesssim 1$. It is precisely at these relatively low redshifts where additional BAO data will be extremely useful.

ACKNOWLEDGMENTS

This work has been supported by the Department of Energy under Contract No. DE-SC0019193. We thank our many collaborators on the DESI analysis team for discussions that have influenced our thinking about the implications of DESI dark-energy results.

DATA AVAILABILITY

The data that support the findings of this article are openly available [1,2,37–41]. Data that are not openly available are available upon reasonable request from the authors.

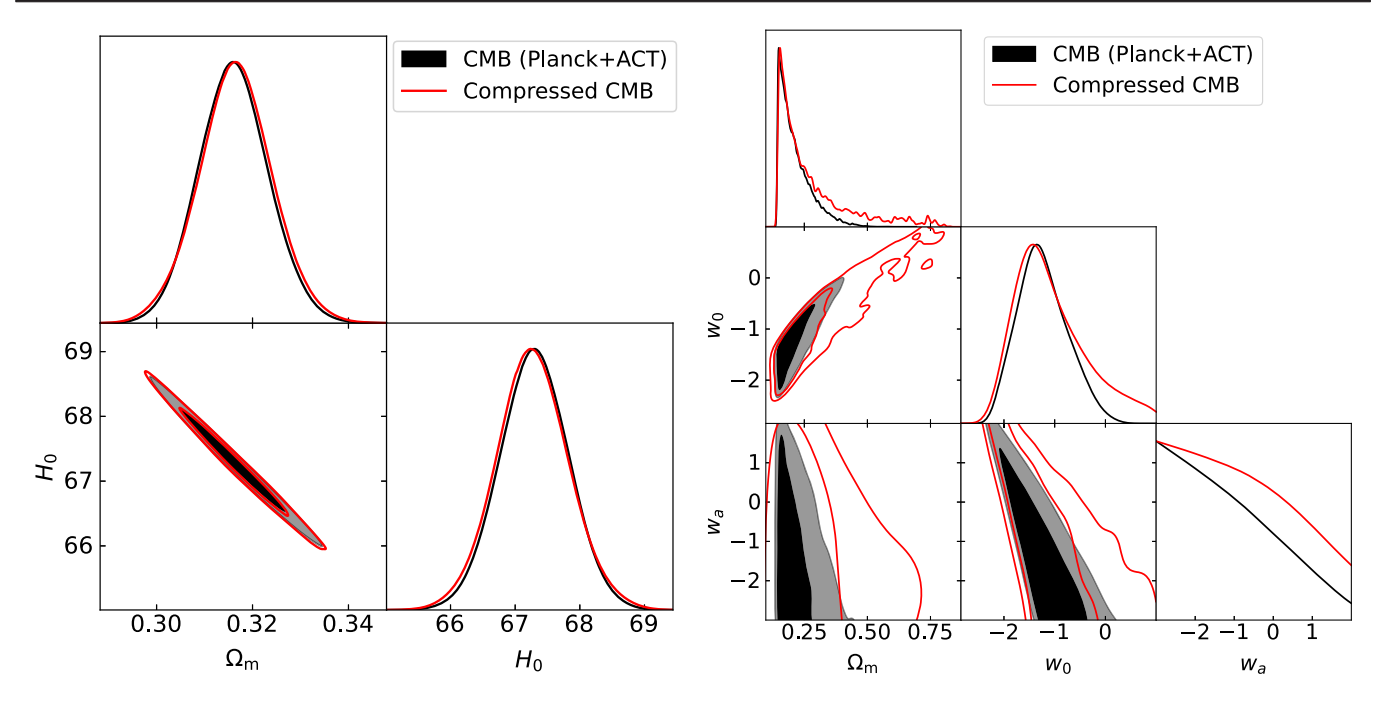


FIG. 3. Comparison of full CMB constraints to those from the compressed CMB datavector in the Λ CDM model (left panel) and w_0w_a CDM model (right panel). Black lines and filled contours show the constraint from the full *Planck* (2018) + ACT (DR6) chain, while the red lines and open contours show the approximate constraints from our compressed data-vector. Note that the constraints in the right panel are poor because we use CMB data alone in this figure, rather than in combination with the BAO.

APPENDIX A: VALIDATION OF THE CMB COMPRESSION

Here we provide more details on the validation of our compressed CMB datavector and its covariance shown in Eqs. (5) and (6).

We obtain the aforementioned compression by considering the joint likelihood that makes use of the PR3 *Planck* PLIK likelihood [37] likelihood [45] and the Data Release 6 of ACT [38]. We next run the MCMC sampler Cobaya [25] on these data. We compute the three-dimensional compressed data-vector and its covariance by running Cobaya on the ΛCDM model. Then, for our validation tests, we use the actual ΛCDM constraints from the aforementioned analysis, and also run Cobaya on the W_0W_aCDM model to get constraints in that parameter space.

For our MCMC chains, we use the default convergence criteria of Gelman and Rubin R statistic < 0.01. To calculate the means, confidence intervals and likelihood distributions for our model parameters, we use the GetDist [26] code with our converged MCMC chains.

Figure 3 shows the comparison of the constraints from the CMB and those derived from our compressed datavector in two cosmological models. In the left panel, we show constraints in Λ CDM with the matter density relative to critical $\Omega_{\rm m}$ and the Hubble constant H_0 as the only free parameters. The agreement between the full Planck (2018) +ACT (DR6) likelihood is excellent, though mostly by construction since our compressed quantities are derived from the Λ CDM MCMC analysis.

A much more convincing validation is obtained with a comparison to another model on which the datavector was not explicitly trained. We adopt the popular phenomenological model that models the equation of state of dark energy as $w(a) = w_0 + w_a(1-a)$, where a is the scale factor and w_0 and w_a are two free parameters. In the right panel of Fig. 3 we compare constraints on the parameter space (Ω_m, w_0, w_a) from the full CMB chain and those derived with our compressed datavector. The agreement is now visually less good, especially in w_a , but note that the principal features of the CMB constraint in this very degenerate parameter space are still reasonably well recovered with the compressed analysis. This bodes well for more realistic cosmological analyses when various datasets will be combined with the CMB in parameter spaces that would be very poorly determined by the CMB alone.

To test this conjectured increased robustness with data of increased constraining strength, we combine the same CMB data [*Planck* (2018) + ACT (DR6)] with the BAO data from the first year of Dark Energy Spectroscopic Instrument (DESI Y1 BAO).⁴ The left panel of Fig. 4 shows

⁴We have explicitly checked that the performance of the compression does not depend on whether we use the DESI BAO data from Data Release 1 or Data Release 2; while we updated the results in the body of this paper with DR2 data [1], we show in these Appendixes the validation with DR1 which we carried out in an earlier version of this paper.

the expected good agreement between the exact and approximate treatment in Λ CDM. The right panel, in turn, shows encouraging results from a much less trivial comparison in the w_0w_a CDM model (on which, recall, the compression was not explicitly trained). We see an excellent agreement between the combined DESI Y1

BAO + CMB results, down to tracing subtle non-Gaussianities in the 2D parameter posteriors.

The results just shown indicate that our compressed datavector faithfully represents the CMB information in cases when nonstandard models affect the expansion history, as, e.g., in the w_0w_a CDM model.

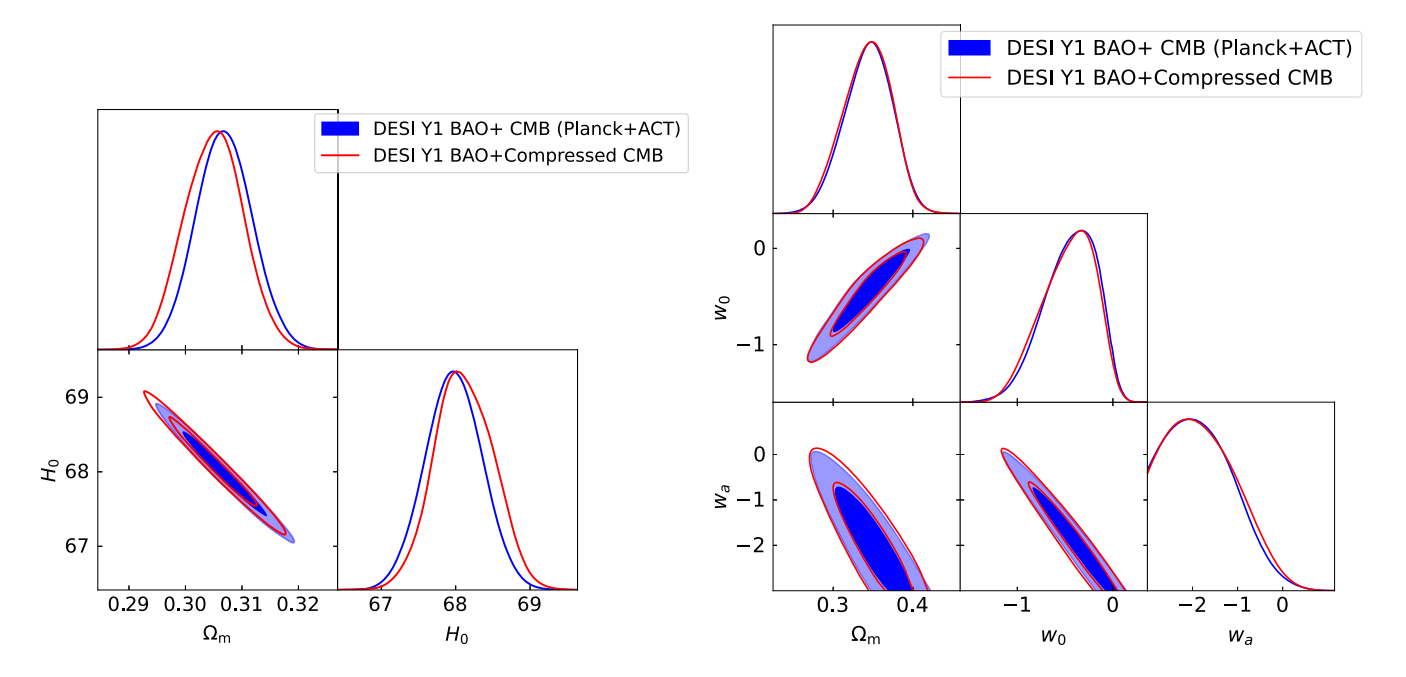


FIG. 4. Comparison of the combined CMB and DESI Y1 BAO constraints in the Λ CDM model (left panel) and the w_0w_a CDM model (right panel) to those obtained when the CMB likelihood is replaced with the compressed datavector and its covariance. The blue lines and filled contours show the constraints when we use the full Planck + ACT chains for the CMB, while the red lines and open contours show the results with our compressed CMB datavector.

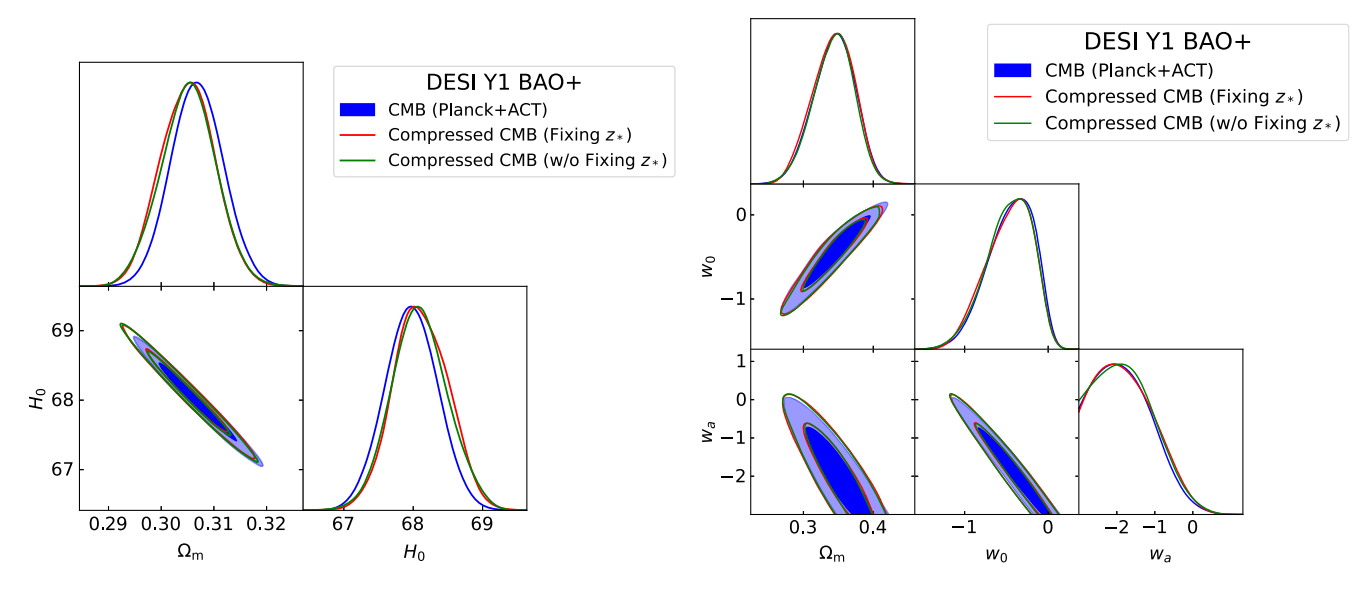


FIG. 5. Comparison of various CMB compression schemes combined with DESI Y1 BAO + constraints in the Λ CDM model (left) and the w_0w_a CDM model (right). The blue filled contours and lines correspond to constraints using the full *Planck* + ACT CMB chains. The red contours show the results using our compressed CMB data vector with z_* fixed, while the green contours use the compressed data vector without fixing z_* .

When computing the compressed CMB datavector and covariance, we fixed the redshift z_* (photon decoupling surface) to 1090 to calculate the means and covariances using the CAMB [46] software. It is natural to question the validity of this assumption, as z_* depends on the expansion history, and hence on the dark-energy model [47]. To address this issue, we recomputed the means and covariances using CAMB without fixing z_* . The derived quantities, RSTAR and DAstar, were calculated directly from CAMB and used to compute R and ℓ_a . Figure 5 compares the constraints obtained using the two approaches for both the Λ CDM and w_0w_a CDM cases. Some references [48–50] have suggested using the approximate expression for z_*

from Hu and Sugiyama [47] for the compressed CMB likelihood. However, these expressions cannot be applied to exotic models that affect the thermal history of the universe. In such cases, our compression proves particularly useful, as it only requires computing the background quantities at $z_* = 1090$ without any additional thermal history calculations to correct z_* .

APPENDIX B: CONSTRAINTS ON THE ALPHAS

Here we provide more detailed information about the constraints on the alpha parameters defined in our modified-H model [see Eq. (1)]. Figure 6 shows the

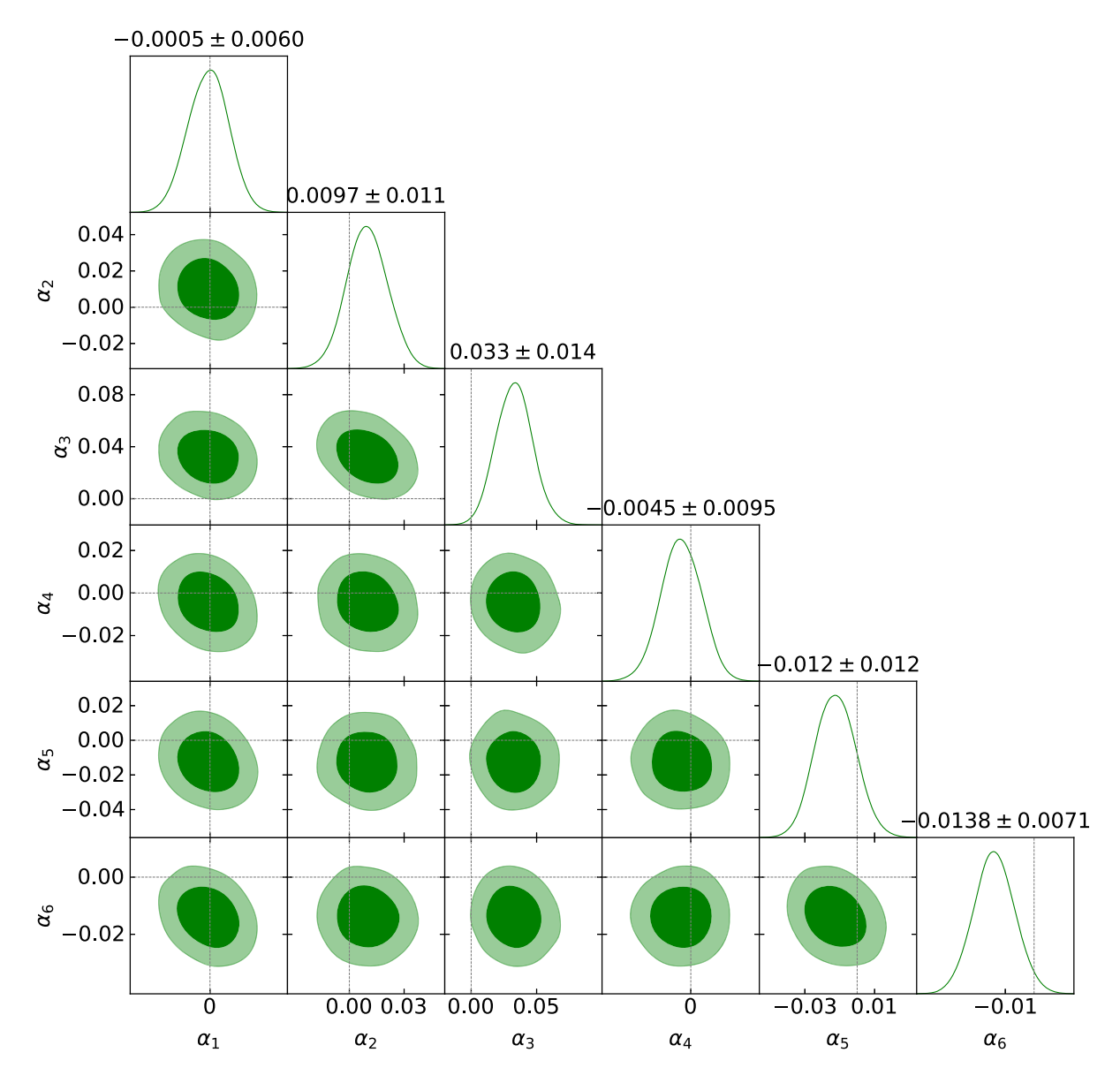


FIG. 6. Constraints on the six parameters that describe perturbations in the Hubble rate [see Eq. (1)], marginalized over the three remaining parameters ($\Omega_b h^2$, $\Omega_{cdm} h^2$ and H_0^{LCDM}). The contours represent the 68.3% and 95.4% credible regions, and the numbers above each diagonal panel shows the projected mean and error in the corresponding alpha. The faint dashed lines are centered at fiducial values in the Λ CDM model, which is zero for each of the alphas.

constraints on the six alpha parameters, marginalized over the three remaining parameters ($\Omega_{\rm b}h^2$, $\Omega_{\rm cdm}h^2$ and $H_0^{\rm LCDM}$), assuming DESI+CMB+DESY5 data, while Table II shows the numerical constraints on all parameters. We see that each of the six alphas is constrained reasonably well; the errors range from 0.01 to 0.04, and this is how well the fractional expansion rate is constrained in the respective redshift bins. Note also that we iterated a little in selecting our flat priors on the alphas in order to ensure that none of the constraints hits the prior boundaries. Table II shows the numerical constraints on all eight parameters of our model, also assuming DESI+CMB+DESY5 data. (For clarity we do not show the constraints with the Union3 or PantheonPlus SNIa datasets.)

We also comment on the calculation of $\Delta \chi^2_{\text{MAP}}$ between the maximum a posteriori (MAP) modified-H and ΛCDM model. This calculation is complicated by the fact that the MAP value for the modified-H model is challenging to locate (standard packages such as IMINUIT fail to find the minimum). We have instead computed these $\Delta\chi^2_{MAP}$ values from the chains, and some further tests indicate that these numbers are reasonably accurate. In addition, we found that the compressed CMB results give slightly different values of $\Delta \chi^2_{\text{MAP}}$ even in cases [e.g., (w_0, w_a) model fits] where the minimization can be carried out. To give an example for the goodness of fit, a combination of DESI Y1 BAO, compressed CMB, and Union3 data (which is also compressed), altogether contain 37 measurements. For our fits with eight free parameters, we expect χ^2_{MAP} of $29 \pm \sqrt{2 \times 29} \simeq 29 \pm 8$, and we observe the best fit of DESI+CMB+Union3 data in the modified-H model to be $\chi^2_{MAP} \simeq 31$.

APPENDIX C: NEUTRINO DENSITY

We have accounted for the neutrino density using the formalism developed in WMAP seven-year analysis [51]

$$\Omega_{\nu}(a) = 0.2271 \Omega_{\gamma}(a) N_{\text{eff}} \left(\frac{1}{3} \sum_{i=1}^{3} f(m_{\nu,i} a / T_{\nu,0}) \right).$$
(C1)

Here $N_{\rm eff}$ is the effective number of neutrino species (fixed at a value 3.044 for this analysis), a is the scale factor, Ω_{γ} is the photon density and $T_{\nu,0}$ is the neutrnio temperature at z=0 (a=1) given by

$$T_{\nu,0} = \left(\frac{4}{11}\right)^{1/3} T_{\text{CMB}} = 1.945 \text{ K.}$$
 (C2)

The function f represents the Fermi-Dirac integral given by

$$f(y) = \frac{120}{7\pi^4} \int_0^\infty \frac{x^2 \sqrt{x^2 + y^2}}{e^x + 1}.$$
 (C3)

To make the code more efficient, we have used the fitting formula [51]

$$f(y) \approx (1 + (Ay)^p)^{1/p}$$
 (C4)

where $A \approx 0.3173$ and p = 1.83.

For the case of two massless neutrinos and one massive neutrino of mass $m_{\nu}=0.06$ eV, the term in the parenthesis in Eq. (C1) simplifies to

$$\frac{1}{3}(2 + f(m_{\nu}a/T_{\nu,0})). \tag{C5}$$

Combining Eq. (C1) with the photon density, we can write the total radiation density (including the contribution from massive neutrinos) as

$$\Omega_{\rm R}(a) = \Omega_{\rm v}(a) + \Omega_{\rm v}(a) \tag{C6}$$

^[1] A. G. Adame *et al.* (DESI Collaboration), J. Cosmol. Astropart. Phys. 02 (2025) 021.

^[2] M. Abdul Karim et al. (DESI Collaboration), arXiv: 2503.14738.

^[3] A. Aghamousa *et al.* (DESI Collaboration), arXiv:1611 .00036.

^[4] B. Abareshi *et al.* (DESI Collaboration), Astron. J. **164**, 207 (2022).

^[5] E. V. Linder, Phys. Rev. Lett. 90, 091301 (2003).

^[6] M. Chevallier and D. Polarski, Int. J. Mod. Phys. D 10, 213 (2001).

^[7] K. Lodha *et al.* (DESI Collaboration), Phys. Rev. D 111, 023532 (2025).

^[8] R. Calderon *et al.* (DESI Collaboration), J. Cosmol. Astropart. Phys. 10 (2024) 048.

^[9] P. Mukherjee and A. A. Sen, Phys. Rev. D **110**, 123502 (2024).

^[10] B. R. Dinda and R. Maartens, J. Cosmol. Astropart. Phys. 01 (2025) 120.

^[11] J. a. Rebouças, D. H. F. de Souza, K. Zhong, V. Miranda, and R. Rosenfeld, J. Cosmol. Astropart. Phys. 02 (2025) 024.

^[12] M. Ishak et al., arXiv:2411.12026.

^[13] A. Chudaykin and M. Kunz, Phys. Rev. D 110, 123524 (2024).

^[14] D. Green and J. Meyers, Phys. Rev. D 111, 083507 (2025).

- [15] W. Elbers, C. S. Frenk, A. Jenkins, B. Li, and S. Pascoli, Phys. Rev. D 111, 063534 (2025).
- [16] M. Cortês and A. R. Liddle, J. Cosmol. Astropart. Phys. 12 (2024) 007.
- [17] K. V. Berghaus, J. A. Kable, and V. Miranda, Phys. Rev. D 110, 103524 (2024).
- [18] C.-G. Park, J. de Cruz Pérez, and B. Ratra, Phys. Rev. D 110, 123533 (2024).
- [19] V. Poulin, T. L. Smith, R. Calderón, and T. Simon, Phys. Rev. D 111, 083552 (2025).
- [20] J.-Q. Jiang, D. Pedrotti, S. S. da Costa, and S. Vagnozzi, Phys. Rev. D 110, 123519 (2024).
- [21] W. J. Wolf, C. García-García, D. J. Bartlett, and P. G. Ferreira, Phys. Rev. D 110, 083528 (2024).
- [22] C.-G. Park, J. de Cruz Perez, and B. Ratra, arXiv: 2410.13627.
- [23] E. V. Linder, arXiv:2410.10981.
- [24] A. Lewis and E. Chamberlain, J. Cosmol. Astropart. Phys. 05 (2025) 065.
- [25] J. Torrado and A. Lewis, J. Cosmol. Astropart. Phys. 05 (2021) 057.
- [26] A. Lewis, arXiv:1910.13970.
- [27] U. Andrade et al. (DESI Collaboration), arXiv:2503.14742.
- [28] L. Casas et al. (DESI Collaboration), arXiv:2503.14741.
- [29] A. G. Adame *et al.* (DESI Collaboration), arXiv:2411 .12022.
- [30] J. R. Bond, G. Efstathiou, and M. Tegmark, Mon. Not. R. Astron. Soc. 291, L33 (1997).
- [31] Y. Wang and P. Mukherjee, Phys. Rev. D 76, 103533 (2007).
- [32] O. Elgaroy and T. Multamaki, Astron. Astrophys. 471, 65 (2007).
- [33] E. Komatsu *et al.* (WMAP Collaboration), Astrophys. J. Suppl. Ser. **192**, 18 (2011).

- [34] M. Vonlanthen, S. Räsänen, and R. Durrer, J. Cosmol. Astropart. Phys. 08 (2010) 023.
- [35] Q.-G. Huang, K. Wang, and S. Wang, J. Cosmol. Astropart. Phys. 12 (2015) 022.
- [36] Z. Zhai, C.-G. Park, Y. Wang, and B. Ratra, J. Cosmol. Astropart. Phys. 07 (2020) 009.
- [37] N. Aghanim *et al.* (Planck Collaboration), Astron. Astrophys. 641, A5 (2020).
- [38] M. S. Madhavacheril *et al.* (ACT Collaboration), Astrophys. J. **962**, 113 (2024).
- [39] T. M. C. Abbott *et al.* (DES Collaboration), Astrophys. J. Lett. **973**, L14 (2024).
- [40] D. Rubin et al., arXiv:2311.12098.
- [41] D. Scolnic et al., Astrophys. J. 938, 113 (2022).
- [42] E. R. Peterson et al., Astrophys. J. 938, 112 (2022).
- [43] R. R. Caldwell and E. V. Linder, Phys. Rev. Lett. 95, 141301 (2005).
- [44] D. Huterer and M. S. Turner, Phys. Rev. D 64, 123527 (2001).
- [45] J. Carron, M. Mirmelstein, and A. Lewis, J. Cosmol. Astropart. Phys. 09 (2022) 039.
- [46] A. Lewis, A. Challinor, and A. Lasenby, Astrophys. J. 538, 473 (2000).
- [47] W. Hu and N. Sugiyama, Astrophys. J. 471, 542 (1996).
- [48] Q. Gao, Z. Peng, S. Gao, and Y. Gong, Universe 11, 10 (2025).
- [49] G. Liu, Y. Wang, and W. Zhao, Phys. Lett. B 854, 138717 (2024).
- [50] R. Lazkoz, V. Salzano, L. Fernandez-Jambrina, and M. Bouhmadi-López, Phys. Dark Universe 45, 101511 (2024).
- [51] E. Komatsu *et al.*, Astrophys. J. Suppl. Ser. **192**, 18 (2011).